

Structural and electronic properties of a sodium tetrasilicate glass from classical and *ab initio* molecular-dynamics simulations.

Simona Ispas*, Magali Benoit, Philippe Jund and Rémi Jullien

Laboratoire des Verres, Université Montpellier II, Place E. Bataillon, 34095 Montpellier, France

(December 2, 2024)

Abstract

The structure and the electronic properties of a sodium tetrasilicate ($\text{Na}_2\text{Si}_4\text{O}_9$) glass were studied by combined Car-Parrinello and classical molecular-dynamics simulations. The glass sample was prepared using a method employed recently in a study of a silica glass [M. Benoit *et al*, Euro. Phys. J. B **13**, 631 (2000)]. First we generated a NS4 glass by classical molecular-dynamics and then we took it as the initial configuration of a first-principles molecular-dynamics simulation. In the *ab initio* molecular-dynamics simulations, the electronic structure was computed in the framework of the Kohn-Sham density functional theory within the generalized gradient approximation using a B-LYP functional. The Car-Parrinello dynamics is remarkably stable during the considered trajectory and, as soon as it is switched on, some significant structural changes occur. The *ab initio* description improves the comparison of the structural characteristics with experimental data, in particular concerning the Si-O and Na-O bond lengths. From an electronic point of view, we find that the introduction of the sodium oxide in the silica network lowers the band gap and leads to a highly non-localized

*Author to whom correspondence should be addressed: ispas@ldv.univ-montp2.fr

effect on the charges of the network atoms.

PACS numbers: 61.43.Bn, 61.43.Fs, 71.15.Pd, 71.23.Cq

1. INTRODUCTION

Over the past three decades, a large number of experimental and theoretical investigations have been carried out in order to extract useful information about the structure and the physical properties of silicate glasses. These materials have stimulated great interest because the advances in understanding them are essential for progress in many scientific fields, such as glass and ceramics chemistry, electronics, earth sciences, or the confinement of industrial and nuclear wastes. However, in spite of their evident importance, there are still important ambiguities in their characterization at a microscopic level. This situation is mainly due to the inherent structural disorder present in glasses which complicates the understanding of the location of the different elements by comparison with crystalline materials.

In view of the current experimental findings and theoretical models, it is generally accepted that the structure of the most common, widely used and intensely studied glass, pure amorphous silica, is composed of SiO_4 tetrahedra which are linked together in a continuous random network by strong bonds of bridging oxygens (BO), i.e. oxygen atoms bonded to two silicon atoms [1]. When a given amount of alkali (Li_2O , Na_2O or K_2O), or alkaline earth (CaO , MgO) metal oxide is incorporated, the connectivity of this network is decreased by the breaking of BO bonds and the formation of non-bridging oxygen atoms (NBO) which are bonded to only one silicon atom and weakly bonded to a cation modifier. Consequently the local environment around the silicon atoms changes depending on the number of bridging oxygen atoms lying within the first shell. This is commonly described by means of the notation Q_n where n is the number of BO atoms linked to a given Si atom ($n=4,3,2,1,0$). From a technological point of view, the introduction of an alkali metal oxide in silica is accompanied by a large reduction of the viscosity, an increase in the thermal expansion coefficient, and a change in the refractive index: these physical properties all depend on the bridging to non-bridging oxygen ratio in the glass [2].

In particular an enormous amount of work has been done on binary sodium silicate glasses since almost all commercial silica glasses and geologic magma are based on this

family of compositions. They may also serve as useful prototypes to interpret the structural and transport properties of more complicated silicate glasses and melts (see for example [3–9] and references therein).

In addition to physical experiments and to advances in techniques such as EXAFS, NMR or XPS, classical molecular-dynamics (MD) simulations have began to provide some insight into the three-dimensional structure of these glasses. However one has to notice that, even though reasonable results have been reported [10–17], this kind of molecular dynamics studies utilizes an interatomic potential generally fixed once and for all throughout the simulation. Moreover it is difficult to adjust a classical potential functional form and parameters which are able to incorporate both a covalent and an ionic character for the bonds existing in the real systems in order to obtain a genuine realistic description. However there exists an alternative approach, the *ab initio* molecular dynamics simulations, where these drawbacks are, in principle, eliminated as the interatomic potential is updated at every simulation step by first principles calculations. The charge transfers between the NBO and the modifier ions can thus be correctly accounted for. Unfortunately one has to pay a price for these obvious advantages, namely a small system size and an extremely limited maximum length of the trajectory.

In this article, we present the microscopic characteristics of a sodium tetrasilicate glass $\text{Na}_2\text{Si}_4\text{O}_9$ (called hereafter NS4) derived from an *ab initio* molecular dynamics simulation. Numerous experimental studies (NMR [18–21], neutron diffraction [22–24], Raman spectroscopies [24,25], XAFS [26,27], ...) have been carried out in order to elucidate the structure and the properties of this glass. The NS4 system has been also analyzed in classical MD calculations [11–14,28] or in reverse Monte Carlo (RMC) fits [24]. The attention given to this system may be justified by the fact that it can be used as a simple model for more complicated aluminosilicate and hydrous silicate glasses.

The present NS4 glass sample was generated using an approach originally employed for obtaining and studying a silica glass sample [29] in two successive steps. First the liquid equilibration, the quench and the glass relaxation are performed classically using a model

potential having the same functional form as the so-called BKS potential (van Best *et al.* [30]) for pure silica. In a second step, the resulting glass configuration is relaxed using the Car-Parrinello (CP) method [31,32]. As in the silica study, a significant amount of CPU time is saved by adopting this strategy since the liquid equilibration, the quench and part of the low temperature relaxation are carried out within the framework of classical MD.

The outline of the paper is as follows: In Sec.2, the methodology is briefly described and the details of the particular simulations performed here are given. In Sec.3, the main results are presented, including structural properties of the NS4 sample in Sec.3A as well as electronic properties in Sec.3B. Section 4 gives the conclusions.

2. SIMULATION DETAILS

We started by generating a liquid sample at a temperature around 3500 K containing 90 atoms (24 silicon atoms, 54 oxygen atoms and 12 sodium atoms) confined in a cubic box of edge length 10.81 Å corresponding to the experimental NS4 mass density of 2.38 g/cm³ [33]. The initial configuration of the NS4 liquid was obtained by melting at 3500 K a β -cristobalite crystal in which SiO_4^{-2} tetrahedra were replaced randomly by $\text{Na}_2\text{O}_3^{-2}$ groups.

For this system we performed classical molecular dynamics simulations within the microcanonical ensemble, with periodic boundary conditions. As mentioned above, we have chosen as the interaction potential a generalization of the BKS potential [30] successfully applied for silica [34] and which was initially developed by Kramer *et al.* [35] in order to study zeolites. Recently Horbach *et al.* [17] have adjusted it for sodium silicate studies by introducing an additional short range term for the sodium ion in order to reproduce the experimental mass density and the structure factor of the sodium disilicate glass.

The NS4 liquid was equilibrated during 70 ps and then cooled from 3500 K to ≈ 300 K at a quench rate of 5×10^{13} K/s, using a time step of 0.7 fs. The cooling procedure used here is identical to the one used in former studies of SiO_2 [29,34] and it has been shown that it gives access to structural, dynamical and thermal properties in good agreement

with experiments. The resulting glass was relaxed during another 70 ps and then the final classical configuration was used as starting point for the Car-Parrinello *ab initio* simulation. Immediately after switching on the CP dynamics we observed a temperature jump similar to the one reported in the silica study [29], which was done following the same approach (see Fig. 1 where the evolution of the ionic temperature is depicted for the end of the classical MD trajectory and the full subsequent CP trajectory). Hence in the CP simulation after a very short relaxation (see the inset of the Fig. 1), the system heats up and then its temperature remains stable around an average value of ≈ 410 K (87 K higher than that of the classical MD simulation).

The CP simulation was performed with the *ab initio* MD code, CPMD developed in Stuttgart [36]. In the *ab initio* MD simulations, the electronic structure was treated via the Kohn-Sham (KS) formulation of density functional theory [37] within the generalized gradient approximation employing the B-LYP functional [38,39]. The KS orbitals were expanded in a plane wave basis at the Γ -point of the supercell up to an energy cutoff of 70 Ry. Core electrons were not treated explicitly but replaced by atomic pseudopotentials of the Goedecker type for silicon [40] and the Troullier-Martins type for oxygen [41], while for sodium a Goedecker type semi-core pseudopotential was employed. Preliminary tests have been performed to check the adequacy of the choices of the pseudopotentials, exchange and correlation functionals and energy cutoff value. The choices of pseudopotentials for Si and O and the energy cutoff value led to a good convergence for the structural properties at 0 K in cristobalite and α quartz. The sodium pseudopotential and exchange and correlation functionals are justified by bond length estimations carried out on Na_2 and Na_2O molecules and which have been found to be close to experimental values [42,43] or more sophisticated theoretical calculations available in the literature [44].

The CP relaxation was performed for ≈ 6 ps, with a time step of 5.5 a.u. (0.13 fs) and a fictitious electronic mass of 800 a.u. used for the integration of the equations of motion. The data have been averaged over the last 5 ps of the trajectory.

The procedure described in the above paragraphs has been carried out a second time

following exactly the same steps and using the same parameters for both BKS and CP simulations, but starting from a different BKS liquid sample. Thus we have generated a second NS4 glass sample which was once again remarkably stable during the CP trajectory after an identical temperature jump showed up at the beginning of the CP simulation. Indeed this second sample heats up from an average temperature of ≈ 315 K at the end of the BKS relaxation to an average CP temperature of ≈ 395 K. Noting that the temperature jumps were of the same order for both samples, we may explain this phenomenon as being due to the fact that under CP, the samples relaxed towards a potential minimum lower than the one calculated during the BKS trajectories and this supplementary potential energy has been transformed into ionic kinetic energy. In the next sections, we will discuss the structural properties obtained by averaging the data collected for both samples during their BKS and CP simulations.

3. RESULTS AND DISCUSSION

A. Structure

In this subsection, we present the structural analysis of both NS4 samples by discussing commonly interrelated features like the pair correlation functions, bond angle distributions, coordination numbers, Q-species distributions, and bridging to non-bridging oxygen ratio. These topics have been investigated for both classical and CP samples in order to understand how much the local arrangement of network formers and modifiers is changed when the system is treated correctly from a quantum mechanical point of view.

We start by remarking that both CP and BKS simulations give the same NBO concentration percentage (22.22%) equal to the sodium-ion concentration which is the value predicted theoretically and confirmed by experiments [20,46]. We have identified the NBO atoms as being either the oxygen atoms having one Si and one Na atom as nearest neighbours or the oxygen atoms having only one Si at a distance below a Si-O bond cutoff (taken

to be 2.0 Å, i.e. where the Si-O pair correlation function becomes zero after the first peak - see below) and we have obtained the same results. Analyzing the neighbourhood of the NBO atoms, we have systematically found that each of these atoms has two Na atoms at almost equal distances, as second and third nearest neighbours. We have also considered the nearest-neighbours of each Si atom and we have found that all Si atoms were coordinated by 4 oxygens during both runs.

Further, once the NBO atoms have been identified, we have determined the Q-species distributions which are equal to 54.2% Q₄, 41.6% Q₃, 4.2% Q₂ for the first sample and to 58.3% Q₄, 33.3% Q₃, 8.3% Q₂ for the second one. We note that the switching on of the CP description did not change these percentages. For the NS4 glass, previous ²⁹Si magic-angle spinning nuclear magnetic resonance experiments reported the following results : 55% Q₄, 40% Q₃, 5% Q₂ by Emerson et al. [19] and 50% Q₄, 48% Q₃, 2% Q₂ by Maekawa et al. [20]. Our simulation results for the first sample compare relatively favorably with the experimental data, while, for the second one, there is an excess of Q₄ and Q₂ species. Nevertheless, in spite of the limited size of the simulated glass and of the ultrafast quench rate, we may point out that there is good overall agreement from the experimental and the simulation data for the Q-species distribution.

From a structural point of view, we note that some significant effects appear as soon as the CP dynamics starts and all of them take place on a very short period of time (\approx 0.1 - 0.2 ps) which can be related to the stabilization time of the temperature. We will examine, in the next paragraphs, each of these effects occurring when switching from the classical to the *ab initio* description and we will discuss the corresponding average structural properties.

1. Mean angles and angular distributions

First, as in the silica glass study [29], an important variation occurs in the mean value of the inter-tetrahedral angle Si-O-Si, which decreases from 146.1° to 141.8° – see Fig. 2(c) which shows the time dependence of the Si-O-Si mean bond-angle during the last 5 ps of the

classical trajectory and the full CP trajectory. Even if the behaviour was similar for both samples, we have chosen to present in Fig. 2 only the data corresponding to one sample. Similarly, in the remaining part of this subsection, all the quantities discussed as a function of time have been plotted for one sample. All the other characteristics have been averaged over both samples.

In Fig. 2(a) and (b), the time dependencies of the O-Si-O and Si-O-Na mean bond-angles during the same time spans are depicted. We can remark that both descriptions give almost identical mean values for the tetrahedral angle O-Si-O, very close to the ideal tetrahedral angle 109.47° . Concerning the Si-O-Na angle, we have computed it taking into account that each NBO has two Na atoms in its nearest neighbourhood as mentioned above. Consequently the depicted values have been taken as the average value of the two corresponding Si-NBO-Na linkages. By looking at the time evolution of the mean value of this angle, we note firstly that it presents a slight shift to a lower value during the CP trajectory. But, since its fluctuations during the CP simulation are slightly larger compared to the BKS ones, we cannot say that the observed shift is a real one without knowing what the origin of these increasing fluctuations is. At first glance, one may think that these increasing fluctuations would be due to the temperature shift. Hence, in order to check this hypothesis, we have classically heated up one of the BKS samples to the CP temperature (i.e. approximately 80 K higher) and let it relax during 70 ps at this new temperature. Neither the mean value of the Si-O-Na angle nor the amplitude of the fluctuations showed any real variation for the heated BKS sample. In view of this result, we cannot interpret the increasing of the Si-O-Na angle fluctuations between the classical and the *ab initio* description as being a temperature effect. They can be much more probably due to the differences in the nearest-neighbour distances observed between the BKS and the CP descriptions (see below). On the other hand, these changes may indicate the fact that the ionicity of the Na-NBO bonds is better described by the CP approach. The Na-NBO bonds are therefore weaker than in the BKS description and this would induce larger fluctuations in the Si-O-Na angle and equally in the Na-NBO mean distances, as we will see in the next paragraphs.

In Fig. 3 we have reported the time-averaged distributions of the tetrahedral O-Si-O and inter-tetrahedral Si-O-Si angles as well as that of the Si-O-Na bond angle, evaluated for both the BKS and CP trajectories. The O-Si-O angular distribution (Fig. 3(a)) shows in both cases a sharp peak at 109° as for the pure silica and this demonstrates that the addition of the sodium oxide does not modify the tetrahedral environment of the Si atoms as was already pointed out from previous classical MD calculations [12,16] and in a RMC fit of the NS4 neutron diffraction data [24]. For the Si-O-Na bond-angle (Fig. 3(b)), we note that both distributions have the same average values (i.e. $120^\circ \pm 19$ in the BKS case and $120^\circ \pm 22$ in the CP one), even if their shapes are not really identical.

From the comparison of the Si-O-Si distributions (Fig. 3(c)), it follows that the CP distribution presents a shift towards lower values, already noticed in the silica study [29] and which is of course consistent with the decrease of the mean angle mentioned above. Nevertheless both distributions have an asymmetric shape as obtained in the recent RMC fits [24] even if their average value ($136^\circ \pm 16$) is slightly lower than those given by the present CP and BKS simulations (i.e. $141^\circ \pm 15$ in the CP case and $145^\circ \pm 15$ in the BKS one). However, in the context of the controversy existing in the literature on the Si-O-Si angle distribution for pure silica as well as for other silicates, we note that the average values given here are comparable with the range of results found up to now by different groups and which lie between 133° and 160° [4,12,16,24,45].

2. First neighbour distances, pair correlation functions and structure factor

The second significant effect mentioned at the beginning of this section and which shows up as soon as the CP simulation starts, concerns the evolution of the mean distances between the Si atoms and their oxygen nearest neighbours. Hence, once the CP dynamics starts, we have noticed, by comparison with the BKS results, an elongation of the mean distances between the Si atoms and their BO nearest neighbours and a shortening of the mean distances between the Si atoms and their NBO nearest neighbours (see Fig. 4). As

can be seen in Fig. 4, these mean distances for the BKS simulated glass have identical values (≈ 1.62 Å) while there exists an important splitting in the CP case which takes place after a very short relaxation (see the inset of same figure) and remains remarkably stable during the whole CP trajectory (the CP Si-BO and Si-NBO mean distances are equal to 1.65 Å and 1.58 Å respectively).

The shortening of the Si-NBO distance and the lengthening of the Si-BO distances are also reflected by the Si-BO and Si-NBO pair correlation functions plotted in Fig. 5. These results are in very good agreement with MD [12] and RMC [24] studies reported for the NS4 glass as well as with the experimental and MD data reported for other crystalline and amorphous sodo-silicates [14,45]. One has to remark that, in the quoted MD simulations [12,14] the authors have used three body potentials while the potential used in the present BKS simulation is a pair potential one. This may be the reason why the quoted MD calculations exhibited different values for the Si-BO and Si-NBO mean distances.

We have also investigated what happens with the mean distance between a NBO atom and its Na nearest neighbour. As shown in Fig. 6, it increases once the CP simulation begins. We recall that two Na atoms have been identified in the nearest neighbourhood of each NBO atom and the values given in Fig. 6 are the averages of the two NBO-Na distances. The lengthening of this distance which occurs also very shortly after the plugging in of the CP description reflects, together with the effects described above, the ability of the CP description to change the local environment around the oxygen atoms even at low temperature.

The pair correlation functions (PCF) $g_{\alpha,\beta}(r)$ ($\alpha, \beta = \text{Si, O, Na}$) and the corresponding integrated coordination numbers (CN) are shown in Fig. 7 for both BKS and CP simulations. We note that the addition of the sodium oxide does not change the positions of the peaks involving the network forming atoms (Si-Si, Si-O and O-O, Fig. 7(a), (b) and (c)) which remain almost the same as those found for pure silica and the two descriptions give overall similar results. Hence the first peaks in the Si-O correlation function exhibit maxima at values of r close to ≈ 1.62 Å, the corresponding experimental value calculated from EXAFS

spectra [47] being 1.617 Å. The Si-O CN being equal to 4, there is no doubt that the SiO₄ tetrahedron remains the basic unit in spite of the presence of the alkali oxide.

When we compare the PCF involving the modifier cation, we note some differences between the results of the BKS and the CP simulations. Firstly, from the analysis of the Na-O PCF (Fig. 7(e)), it follows that the BKS Na-O first peak is located at ≈ 2.2 Å while the CP one at ≈ 2.3 Å. This shift of the average first neighbour Na-O distance towards higher values of r in the CP description is of course consistent with the increase observed in the time evolution of the NBO-Na mean distance (see Fig. 6). The CP average first neighbour Na-O distance shows a very good agreement with previous XAFS measurements [26,27] which gave an average value of 2.32 Å.

Concerning the Si-Na PCF (Fig. 7(d)), we can notice that its shape is not similar for the classical and *ab initio* descriptions. After an almost identical first peak located at ≈ 3.4 Å, the BKS function presents a kind of plateau for r varying from ≈ 4 to 4.8 Å. During the CP simulation, one can see that this plateau disappears. Since this plateau is more pronounced in one of the two BKS samples, it could simply be an artifact of the unrealistic quench rates that one has to impose usually in MD simulations. On the other hand, this plateau has been observed also in a classical MD simulation using the same BKS potential for one NS4 sample containing 648 atoms [48] which shows that it is not due to finite size effects. The first peak position obtained here is in agreement with the RMC [24] fits and previous classical MD results [12,16], but it is lower than that estimated from sodium K-edge XAFS experiments (i.e. 3.8 Å) [26,27].

From the same XAFS experiments [26,27], the Na-Na average distance have been refined at 3.2 Å. In the present work, the first peak of the Na-Na PCF has a maximum at ≈ 3 Å for both BKS and CP case (see Fig. 7(f)). In the BKS case, the Na-Na PCF shows a splitting which seems to be smoothed in the CP case. However, it is difficult to extract really useful information concerning the Na-Na correlation given the poor statistics which is due to the small number of Na atoms in the system.

Figure 8 shows the total static structure factor computed from the CP and BKS simulations compared with the experimental points that we have extracted from a neutron diffraction experiment [24]. The differences between the curves corresponding to the two simulations are indistinguishable and they agree reasonably with experimental data. Nevertheless it is interesting to notice that the microscopic discrepancies between the two descriptions, reported above, are totally smoothed out in the total structure factor. Thus, the good agreement shown by the $S(q)$ is not sufficient to draw conclusions on the validity of a model and a more detailed analysis of the structure is required.

B. Electronic properties

In this subsection, we analyze the electronic properties of the two NS4 *ab initio* samples in terms of the electronic density of states and the Hirshfeld charge variations. These properties were computed for the final configurations of the CP runs and compared to the ones obtained for the initial configurations (corresponding to the final configurations of the classical BKS simulations). We compare the corresponding NS4 results with those obtained for the *ab initio* silica glass sample described in Ref. [29].

1. Electronic density of states

The Kohn-Sham (KS) eigenvalues are computed for both NS4 samples and the resulting electronic density of states (DOS) is depicted in Fig. 9(a) for the initial configurations of the CP runs, and in Fig. 9(b) for the final ones. In Fig. 9(b), the KS densities of states for NS4 are compared to the density of states of the silica glass sample studied in Ref. [29]. However, since the present NS4 study has been carried out using the LDA-B-LYP functional for the exchange and correlation energy term, we have also computed the KS eigenvalues of the silica glass using the same approximation (these eigenvalues were originally computed within the LDA description in Ref. [29]). We have found only very slight differences between the SiO₂ DOS using LDA and LDA+B-LYP. At ≈ 335 K, the band gap is found to be equal

to 5.01 eV with the LDA+B-LYP description, which is much lower than the experimental value for amorphous silica (≈ 9 eV). This underestimation of the band gap is a well-known failure of DFT in the local density approximation [49].

The band gaps obtained for the two NS4 samples at ≈ 400 K are equal to 2.77 eV and to 2.86 eV, respectively (Fig. 9(b)). For comparison, the band gaps obtained for these two samples in their initial configurations were equal to 2.16 eV and 2.17 eV, respectively (Fig. 9(a)). Hence, the refinement of the NS4 glass structure by the Car-Parrinello dynamics leads to an increase of the band gap. By comparing with the value obtained for the silica glass, we note that the gap is significantly reduced by the introduction of Na atoms, as had already been deduced from UV absorption experiments [50,51] and suggested in LCAO calculations [52].

The DOS for the two NS4 samples are very similar and show common features with the DOS of SiO_2 (Fig. 9(b)). They mainly consist in oxygen $2p$ non bonding orbitals (lone pair) for the highest occupied states, in bonding states between silicon sp^3 hybrids and oxygen $2p$ orbitals (from -10 eV to -4 eV for SiO_2 and from -11 eV to -5.4 eV for NS4) and in oxygen $2s$ orbitals for the lower energy band. The empty band is mainly derived from weak anti-bonding conduction states. Note that in our NS4 samples, we take explicitly into account semi-core electrons for the Na atoms. These electrons give rise to a low energy band at ≈ -48 eV which has not been considered in Fig. 9.

Murray *et al.* [52] computed the DOS for sodium silicate model glasses with various compositions, using a LCAO computational method. Since they used atomic orbitals in their model, they could assign different contributions in the bands to states belonging to specific atoms. For instance, the NBO atoms gave rise to subpeaks or shoulders to the right of the main O $2s$ and O $2p$ bands. In the Kohn-Sham description, the orbitals are not atomic orbitals and consequently such an analysis of the bands is not possible. However, from the comparison of our DOS and the DOS reported in Ref. [52], we note that they are surprisingly similar and therefore, we can attribute the peak just below the Fermi level and the peak at ≈ -16.5 eV to the NBO atoms. In Ref. [53], the reported value for the chemical

shift between the BO and the NBO 1s-photoelectron bands measured by XPS experiments was about 2.45 eV. We find values of ≈ 2.5 eV for the O 2s bands and of ≈ 2.0 eV for the O 2p bands.

By comparison, the bands for the initial configurations - corresponding to the structure given by the BKS potential (Fig. 9(a)) - show only very slight differences with the bands computed at the end of the CP runs. The O 2s bands are slightly modified and the peak just below the Fermi level attributed to the NBO atoms seems to be shifted towards lower values after the CP structure refinement. This is consistent with the Si-NBO bond length shortening that occurs after the CP is switched on.

2. Atomic charges

It is well-known that the charge of an atom can never been defined uniquely and it is not subject to experimental measurement. Nevertheless, it is possible to use approaches such as Mulliken population analysis [54] or Hirshfeld determination of the density deformation [55] in order to discuss bonding or to compare the electron distributions in different systems using the same description. Here we have chosen to use the Hirshfeld description to determine variations of the atomic charges between the NS4 samples and the silica samples. In this scheme, the total electronic charge of a bonded atom is given by:

$$\mathcal{Q}_i = - \int \delta\rho_i(r)dv$$

where $\delta\rho(r)$ is the atomic deformation density, defined as the difference between what Hirshfeld calls the "charge density of the bonded atom" and the "atomic density", i.e. the density difference between the free atom and the bonded atom (see Ref. [55] for a more complete definition). Adding the charge of the nucleus Z_i gives the net atomic charge:

$$q_i = \mathcal{Q}_i + Z_i.$$

This description, based on the integration of the atomic deformation densities, has been used to compute atomic charges [55] that appear reasonable in magnitude and show variations

consistent with the accepted ideas about electronegativity differences between atoms and groups. However, the absolute values obtained using this approach tend to be smaller than values obtained by other methods, such as Mulliken analysis, and only variations of these charges have been examined here. The calculations have been performed at 0 K with fully optimized structures in the LDA+B-LYP description and the results are presented in Table I.

By comparing the Hirshfeld net charges obtained in the two NS4 samples, we first notice that the values are extremely similar, the differences being within the error bars. We have also compared these charges with the ones computed on the initial configuration of the two CP runs and we have observed no significant differences, given the large error bars.

In the NS4 glasses, the charges on the NBO atoms are, on average, more negative than the ones on the BO atoms, which is a generally admitted result. Moreover we note that the differences between the charges on the silicon atoms depend on the character of the tetrahedra (Q_n). The positive charge on the silicon atoms decreases as n decreases, i.e. the proximity of the NBO and of the Na atoms has a direct effect on the silicon atom and thus on the tetrahedra. This effect is known as a "non-localized effect" of the Na atom on the silica network [51,53,56] and has already been shown in *ab initio* molecular orbitals calculations on sodium silicate clusters [51,56]. But even if the electronic properties of the clusters were in agreement with experimental results from UV absorption and XPS measurements [50,53], some of the geometrical features were not correctly reproduced (in particular NBO-Na bond lengths). In our simulation, this "non-localized effect" gives rise to the increase of the Si-BO bond length and to the decrease of the Si-NBO one (as presented in subsection 3 A), while the Na-NBO bond length is in agreement with experimental values. We also observe that the increase of the Si-BO bond length is more pronounced in Q_3 and Q_2 tetrahedra than in Q_4 tetrahedra, in parallel with the increase of the Si net charges.

On the other hand, comparison of the average charges found on the BO atoms between the NS4 samples and the SiO_2 sample shows that the BO atoms in SiO_2 have a more negative charge than the BO atoms in NS4. As a direct consequence, the Si atoms in SiO_2 are less

charged than the corresponding Si atoms in the Q_4 conformation in the NS4 samples. This effect is also very probably a consequence of the highly non-localized effect of the Na atoms on the silica network.

4. CONCLUSION

We have presented a structural and electronic analysis of a sodium tetrasilicate (NS4) glass by using a combination of classical and *ab initio* molecular dynamics simulations. The electronic structure has been computed in the framework of the Kohn-Sham density functional theory within the generalized gradient approximation using a B-LYP functional. To our knowledge, this is the first study of a binary silicate glass carried out in the frame of first-principles molecular dynamics calculations.

The scheme employed for the preparation of the *ab initio* NS4 samples economizes a considerable amount of computation time as was already shown in recent work on the structural and electronic properties of a silica glass [29]. As in the silica study, the CP dynamics has presented a remarkable stability. In order to validate this approach, we have performed it twice and we have obtained the same behavior both times.

The structural features of the NS4 samples have been studied in terms of pair correlation functions, bond angle distributions, Q-species, bridging to non-bridging oxygen ratio and structure factor. We note that, once the CP dynamics was plugged in, some important structural changes occurred. Hence the shortening of the Si-NBO distance, the lengthening of the Si-BO and Na-NBO distances appearing immediately after the start of the CP simulation are in perfect agreement with the experimental data. These results validate our preparation method and show the ability of the CP description to refine the local environment of the atoms even at low temperature.

The electronic structure of the *ab initio* samples thus obtained has been analyzed in terms of the density of states and the atomic charge variations. The results show that the introduction of sodium atoms into the silica network lowers the band gap and that it has a

highly non-localized effect on the charges of the atoms in the network.

In conclusion, we have generated - at low computational cost - a fully *ab initio* sodium tetrasilicate glass which shows structural and electronic characteristics in very good agreement with experimental results. This work is a first step towards accurate studies of detailed electronic and vibrational properties of the sodium tetrasilicate glass.

ACKNOWLEDGMENTS

We would like to thank Walter Kob and Mark Tuckerman for very interesting and stimulating discussions and Jürg Hutter for his invaluable help with the CPMD code. The simulations have been performed on the IBM/SP2 and IBM/SP3 in CINES, Montpellier FRANCE.

REFERENCES

- [1] *The Physic and Technology of Amorphous SiO₂*, edited by R. A.B. Devine, Plenum Press, New York (1988).
- [2] B. O. Mysen, *Structure and properties of Silicate Melts*, Elsevier, Amsterdam (1988).
- [3] S. A. Brawer and W.B. White, J. Non-Cryst. Sol. **23**, 261 (1977).
- [4] G. N. Greaves, A. Fontaine, P. Lagarde, D. Raoux and S.J. Gurman, Nature **293**, 611 (1981).
- [5] G. N. Greaves, J. Non-Cryst. Sol. **71**, 203 (1985) ; G. N. Greaves, S.J. Gurman, C. R. A. Catlow, A. V. Chadwick, S. Houde-Walter, C. M. B. Henderson and B. R. Dobson, Phil. Mag. A **64**, 1059 (1991) ; G. N. Greaves, Solid St. Ionics **105**, 243 (1998) ; G. N. Greaves, Miner. Mag. **64**, 441 (2000).
- [6] G. E. Brown, F. Farges and G. Calas, in *Reviews in Mineralogy*, **32**, ed. J.F. Stebbins, P. F. McMillan and D. G. Dingwell, 317 (1995).
- [7] S. A. Brawer and W.B. White, J. Chem. Phys. **63**, 2421 (1974).
- [8] T. Furukawa, K.E. Fox and W.B. White, J. Chem. Phys. **75**, 326 (1981).
- [9] C. Mazzara, J. Jupille, A.-M. Flank and P.Lagarde, J. Phys. Chem. B **104**, 3438 (2000).
- [10] T. F. Soules and R. F. Busbey, J. Chem. Phys. **75**, 969 (1981).
- [11] A. A. Tesar and A. K. Varshneya, J. Chem. Phys. **87**, 2986 (1987).
- [12] C. Huang and A. N. Cormack, J. Chem. Phys. **93**, 8180 (1990).
- [13] C. Huang and A. N. Cormack, J. Chem. Phys. **95**, 3634 (1991).
- [14] H. Melman and S. H. Garofalini, J. Non-Cryst. Sol. **134**, 107 (1991).
- [15] W. Smith, G. N. Greaves and M. J. Gillan, J. Chem. Phys. **103**, 3091 (1995).

- [16] J. Oviedo and F. Sanz, Phys. Rev. B **58**, 9047 (1998).
- [17] J. Horbach, W. Kob & K. Binder, Chem. Geol. **174**, 87 (2001).
- [18] R. Dupree, D. Holland, P.W. McMillan and R.F. Pettifer, J. Non-Cryst. Sol. **68**, 399 (1984).
- [19] J. F. Emerson, P.E. Stallworth and P.J. Bray, J. Non-Cryst. Sol. **113**, 253 (1989).
- [20] H. Maekawa, T. Maekawa, K. Kawamura and T. Yokokawa, J. Non-Cryst. Sol. **127**, 53 (1991).
- [21] J. Kümmerlen, L. H. Merwin, A. Sebald and H. Keppler, J. Phys. Chem. **96**, 6405 (1992).
- [22] N. Zotov, H. Keppler, A.C. Hannon and A.K. Soper, J. Non-Cryst. Sol. **202**, 153 (1996).
- [23] N. Zotov and H. Keppler, Phys. Chem. Minerals **26**, 107 (1998).
- [24] N. Zotov and H. Keppler, Phys. Chem. Minerals **25**, 259 (1998).
- [25] G. H. Wolf, D.J. Durben and P. F. Mc Millan, J. Chem. Phys. **93**, 2280 (1990).
- [26] S.N. Houde-Walter, J.M. Inman, A.J. Dent and G. N. Greaves, J. Phys. Chem. **97**, 9330 (1993).
- [27] G. N. Greaves and K.L. Ngai, Phys. Rev. B **52**, 6358 (1995).
- [28] N. Zotov, I. Ebbsjö, D.Timpel and H. Keppler, Phys. Rev B **60**, 6383 (1999).
- [29] M. Benoit, S. Ispas, P. Jund and R. Jullien, Euro. Phys. J. B **13**, 631 (2000).
- [30] B.W. H.van Best, G.J. Kramer & R.A. van Santen, Phys. Rev. Lett. **64**, 1955 (1990).
- [31] R. Car and M. Parrinello, Phys. Rev. Lett. **55**, 2471 (1985).
- [32] D. Marx and J. Hutter, in *Modern methods and Algorithms of Quantum Chemistry*, ed. J. Grotendorst, Forshungszentrum Jülich, NIC Series, **1**, 301 (2000).

- [33] N. P. Bansal and R. H. Doremus, *Handbook of Glass Properties*, Academic Press, INC., New York (1986).
- [34] K. Vollmayr, W. Kob & K. Binder, Phys. Rev. B **54**, 15808 (1996); P. Jund & R. Jullien, Phys. Rev. B **59**, 13707 (1999); P. Jund & R. Jullien, Phil. Mag. A **79**, 233 (1999)
- [35] G.J. Kramer, A.J.M. de Man & R.A. van Santen, J. Am. Chem. Soc. **64**, 6435 (1991)
- [36] CPMD Version 3.3, J. Hutter, A. Alavi, T. Deutsch, M. Bernasconi, S. Goedecker, D. Marx, M. Tuckerman & M. Parrinello, MPI für Festkörperforschung & IBM Zurich Research Laboratory (1995-99).
- [37] W. Kohn and L. Sham, Phys. Rev. **140 A**, 1133 (1965).
- [38] A.D. Becke, Phys. Rev. A **38**, 3098 (1988).
- [39] C. Lee, W. Yang and R.G. Parr, Phys. Rev. B **37**, 785 (1988).
- [40] S. Goedecker, M. Teter and J. Hutter, Phys. Rev. B **54**, 1703 (1996).
- [41] N. Trouiller and J.L Martins, Phys. Rev. B **43**, 1993 (1991).
- [42] K. P. Huber and G. Herzberg, *Constants of Diatomic Molecules*, Van Nostrand Reinhold, New York (1979).
- [43] P.L. Silvestrelli, A. Alavi and M. Parrinello, Phys. Rev. B **55**, 15515 (1997).
- [44] S.D. Elliott and R. Ahlrichs, J. Chem. Phys. **109**, 4267 (1998).
- [45] W. S. McDonald and D.W.J. Cruickshank, Acta Cryst. **62**, 37 (1967).
- [46] J. S. Jen and M.R. Kalinowski, J. Non-Cryst. Solids **38 - 30**, 21 (1989).
- [47] G. S. Henderson, J. Non-Cryst. Solids **183**, 43 (1995).
- [48] E. Sunyer and P. Jund, private communication.
- [49] R.W. Godby, M. Schlüter, L.J. Sham, Phys. Rev. B **37**, 10 (1988).

- [50] G.H. Sigel, Jr., J.Non-Cryst. Solids **13**, 372 (1973/74).
- [51] T. Uchino, M. Iwasaki, T. Sakka and I. Ogata, J. Phys. Chem. **95**, 5455 (1991).
- [52] R.A. Murray and W.Y. Ching, J. Non-Cryst. Solids **94**, 144 (1987).
- [53] R. Brückner, H.-U. Chun, H. Goretzki, M. Sammet, J.Non-Cryst. Solids **42**, 49 (1980).
- [54] R. S. Mulliken, J. Chem. Phys. **23**, 1833 (1955).
- [55] F.L. Hirshfeld, Theor. Chim. Acta **44**, 129 (1977)
- [56] T. Uchino, T. Sakka, I. Ogata and M. Iwasaki, J. Phys. Chem. **97**, 9642 (1993).

FIGURES

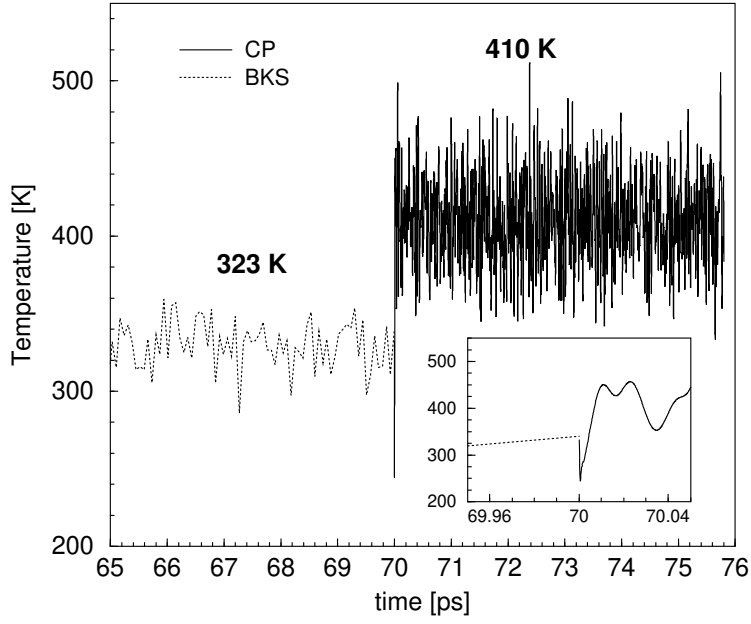


FIG. 1. Ionic temperature evolution during the last 5 ps of the classical MD simulation (dotted line) and the full Car-Parrinello MD simulation (solid line). In the inset, a zoom of the beginning of the Car-Parrinello MD simulation is depicted.

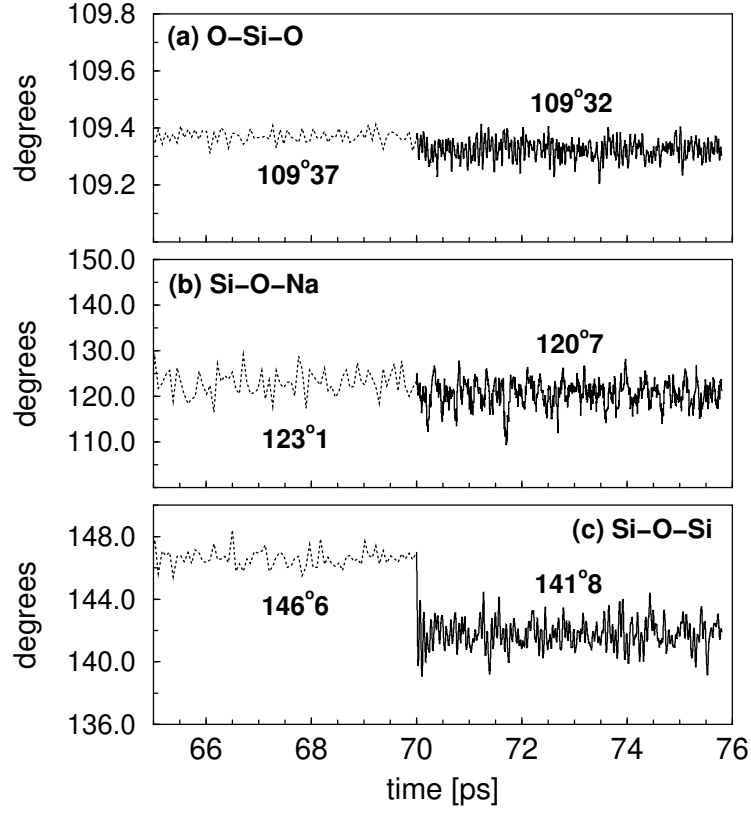


FIG. 2. Time evolution of the mean O-Si-O (a), Si-O-Na (b) and Si-O-Si (c) bond angles during the last 5 ps of the classical MD simulation (dotted lines) and the full Car-Parrinello MD simulation (solid lines).

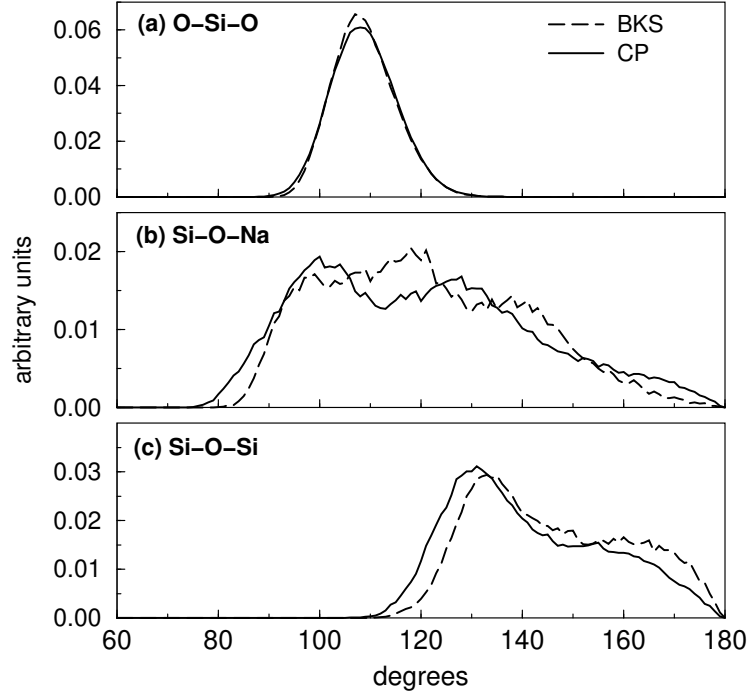


FIG. 3. The O-Si-O (a), Si-O-Na (b) and Si-O-Si (c) time-averaged angle distributions from the Car-Parrinello MD simulation (solid line) and from the classical MD simulation (long dashed line), respectively.

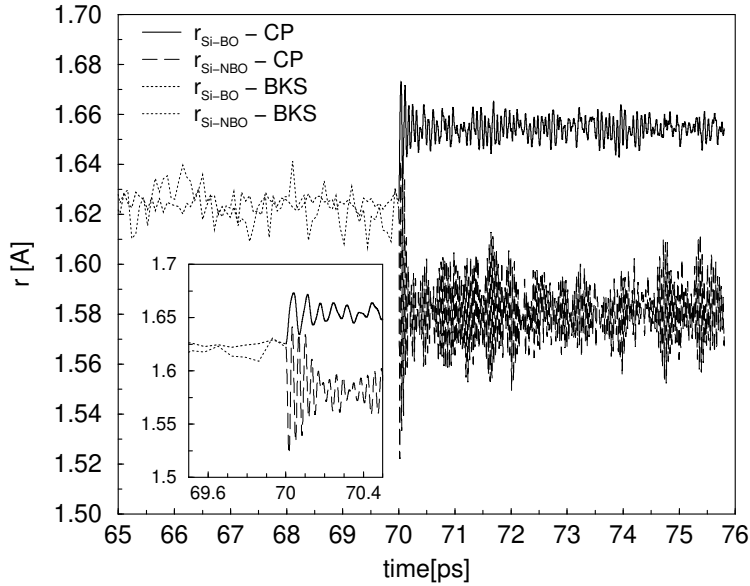


FIG. 4. Time evolution of the Si-BO and Si-NBO mean distances during the last 5 ps of the classical MD simulation and the full Car-Parrinello MD simulation.

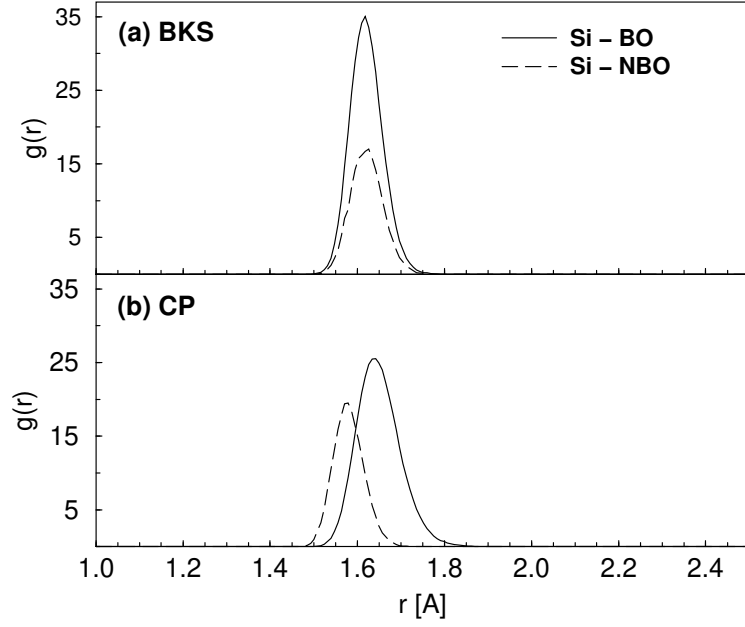


FIG. 5. First peaks of the Si-BO (solid line) and Si-NBO (dashed line) pair correlation functions of the NS4 glass computed from the classical MD (a) and the Car-Parrinello MD (b) simulations.

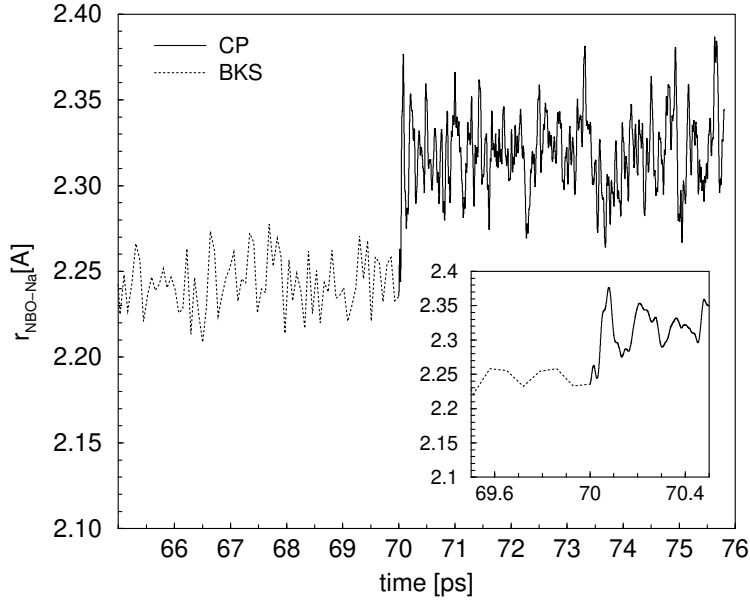


FIG. 6. Time evolution of the NBO-Na mean distances during the last 5 ps of the classical MD simulation (dashed line) and the full Car-Parrinello MD simulation (solid line).

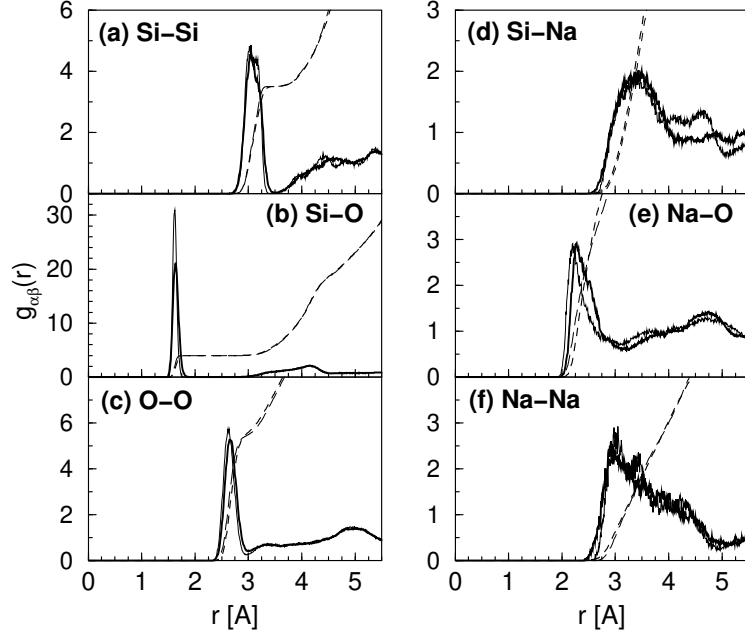


FIG. 7. Pair correlation functions of the NS4 glass obtained from the Car-Parrinello MD (bold solid lines) and classical MD (thin solid lines) simulations. The bold dashed and the thin long-dashed lines are the corresponding integrated coordination numbers.

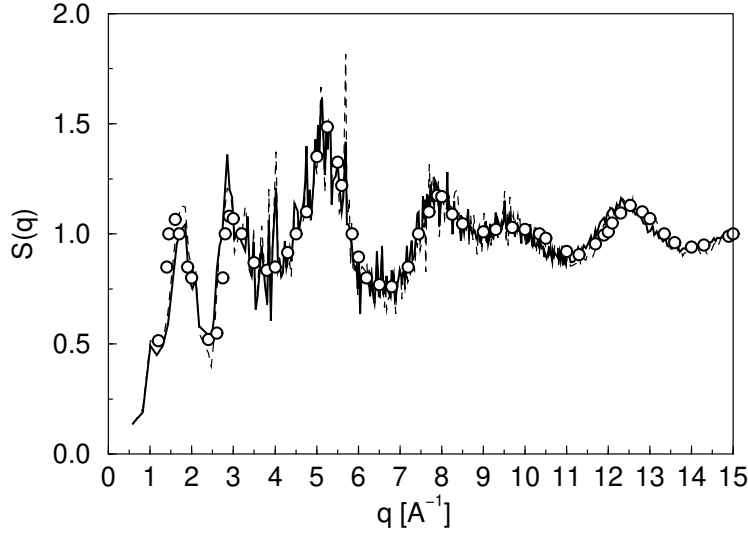


FIG. 8. Comparison between the experimental neutron diffraction structure factor (the circles) that we have extracted from reference [24] and the computed static structure factors from Car-Parrinello MD (solid line) and classical MD (dotted line) simulations. For the calculations of the structure factors, the scattering lengths $b_{Si} = 4.149 \text{ Å}$, $b_O = 5.803 \text{ Å}$ and $b_{Na} = 3.63 \text{ Å}$ were used.

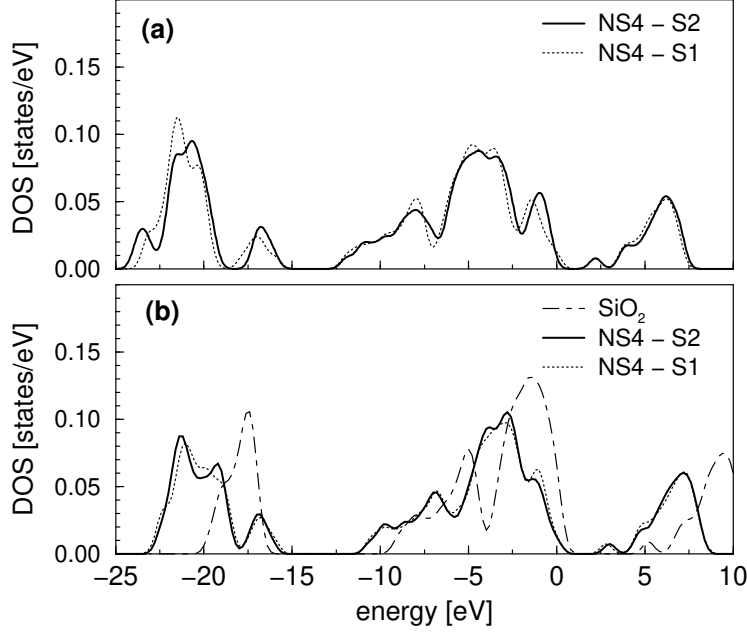


FIG. 9. Upper graph: Kohn-Sham electronic density of states of the initial CP configuration of the two NS4 samples at ≈ 300 K, corresponding to the last configuration of the BKS simulations, denoted S1 and S2 (solid and dotted lines). Lower graph: Kohn-Sham electronic density of states of the last CP configuration of the two NS4 samples at ≈ 400 K, denoted S1 and S2 (solid and dotted lines) compared to the SiO_2 density of states of Ref. [29] at ≈ 335 K (dotted-dashed line). The Fermi levels have been shifted to zero and the curves have been smoothed with a Gaussian broadening of same width.

TABLES

	Na ₂ O-4SiO ₂		SiO ₂
	sample 1	sample 2	sample from Ref [29]
BO	-0.089 ± 0.009	-0.089 ± 0.011	-0.109 ± 0.007
NBO	-0.249 ± 0.015	-0.245 ± 0.020	-
Na	0.082 ± 0.034	0.076 ± 0.038	-
Si (all atoms)	0.240 ± 0.041	0.240 ± 0.035	0.218 ± 0.010
Si (Q_4)	0.270 ± 0.012	0.262 ± 0.017	0.218 ± 0.010
Si (Q_3)	0.212 ± 0.022	0.222 ± 0.012	-
Si (Q_2)	0.153 ± 0.005	0.125	-

TABLE I. Average Hirshfeld atomic net charges computed from the fully optimized structures of the two NS4 samples and of the SiO₂ sample of Ref. [29] at 0 K.